Subcloud and cloud base vertical velocity and water vapor anomalies during shallow cumulus convection

University of Nevada, Reno

ASR Atmospheric System Research

Neil P. Lareau, Department of Physics, University of Nevada, Reno, email: nlareau@unr.edu

1. The importance of latent heat fluxes

Motivation: Entrainment and cloud base latent heat fluxes are infrequently observed and incompletely understood, yet strongly impact boundary layer humidity budgets and cloud development.

Our approach: Co-located Doppler and Raman lidars at ARM-SGP are used to simultaneously sample vertical velocity and water vapor mixing ratio to compute the latent heat flux profile (**w'q'**) during days with shallow cumulus convection

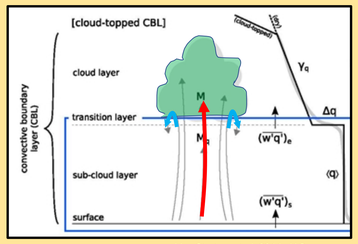

Van Stratum et al. 2014, JAS

Cloud bases fluxes of mass ($\rho w'$) and moisture ($w'q'$)

2. Doppler and Raman Lidar Data

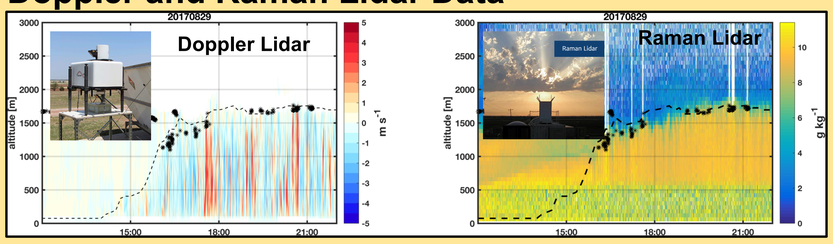

- **Doppler Lidar (DL):** IR laser sensitive to aerosol backscatter:
  - Vertical velocity/Aerosol Backscatter
  - Cloud base/edge detections
  - 1 sec temporal resolution
- **Raman Lidar (RL):** UV laser sensitive to molecular and aerosol backscatter:
  - Water-vapor mixing ratio
  - Cloud base/edge detections,
  - 10 second temporal resolution

- Data are drawn from a sample of 20 days at ARM-SGP with shallow cumulus convection

3. Adaptive Data Filtering and Flux Computation

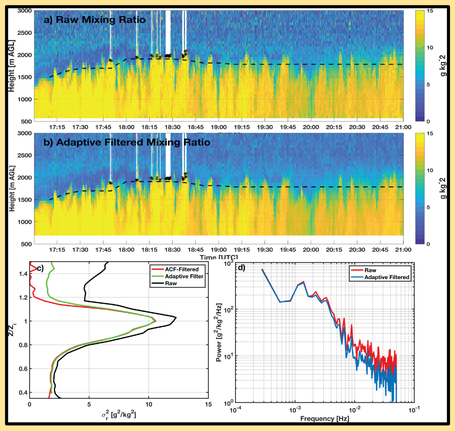

Process level details are preserved using an adaptive image filtering technique (see handout) informed by the autocovariance noise estimate. The quantitative and qualitative aspects of this filtering is demonstrated in Fig. 1.

Fig. 1 (a) Raw RL water vapor mixing ratio. (b) data passed through an adaptive noise filter. (c) Water vapor variance profiles from the raw (black), auto-covariance filtered (ACF; red), and adaptive noise filter (green). (d) Power spectra for the raw and adaptive noise filtered data.

Vertical velocity (w') and water vapor mixing ratio (q') anomalies (Fig. 2) are used to compute the latent heat flux profile for overlapping 30 minute increments:

$$LH = \rho L_v \overline{w'q'}$$

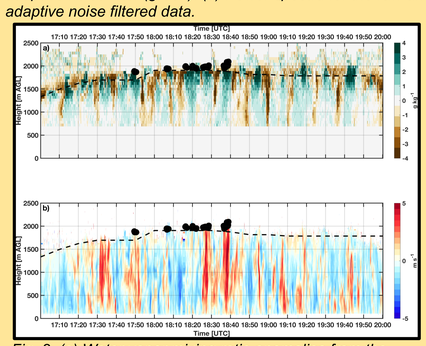

Fig. 2. (a) Water vapor mixing ratio anomalies from the adaptively filtered RL data . (b) Vertical velocity from the Doppler lidar. Shown in each panel are the CBL heights (dashed line) and cloud-base detections (black dots).

4. Mean and Variance Profiles

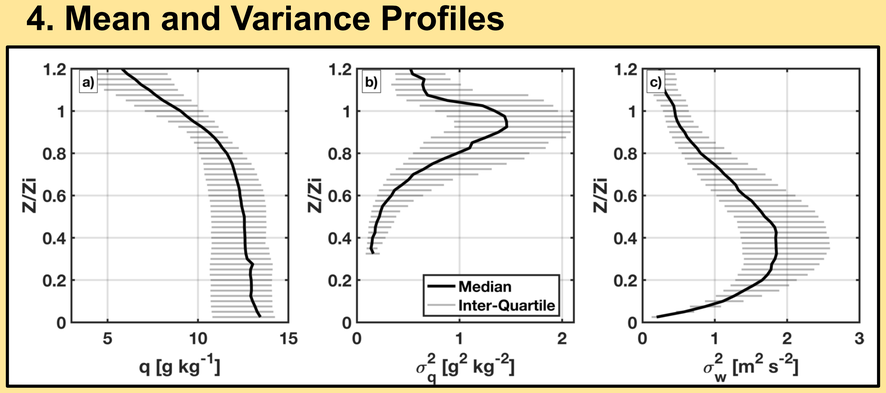

Fig. 3 Water vapor mixing ratio and vertical velocity statistics. (a) Median and interquartile range of the height-normalized water vapor mixing ratio profiles. (b) Median and interquartile range of water vapor mixing ratio variance profile. (c) Median and interquartile range of vertical velocity variance profile. The height normalization is by the CBL height, Z_i.

Mean Mixing Ratio (Fig. 3a): Well-mixed with a sharp drop in mixing ratio across CBL top.

Mixing Ratio Variance (Fig 3b): Low variance in the lower 2/3 of the CBL. Peak variance near 0.9Z_i corresponding to updrafts and downdrafts perturbing the mean gradient.

Vertical Velocity Variance (Fig. 3c): Variance peaks near 0.4Z_i

Vertical Velocity Skewness (not shown): Strongly positively skewed, peaking in the upper CBL

5. Latent Heat Flux Profiles

- Latent heat flux increases quasi-linearly with height from the surface to ~0.8Z_i.
- Flux decreases from 0.8-1Z_i
- Varying magnitude of flux divergence dries the CBL
- Fluxes vary with cloud fraction:
  - Higher cloud fractions are linked to larger fluxes in the upper CBL

Figure 4. (a) Median, interquartile, and 10-90% range of latent heat fluxes. Also shown are the surface fluxes for the same statistical ranges. A line connecting the surface fluxes to the fluxes aloft is shown for each statistical range. (b) Latent heat flux profiles stratified by cloud fraction (CF). The dots indicate statistically significant differences. The inset shows the distribution of cloud fraction amongst the cloudy profiles.

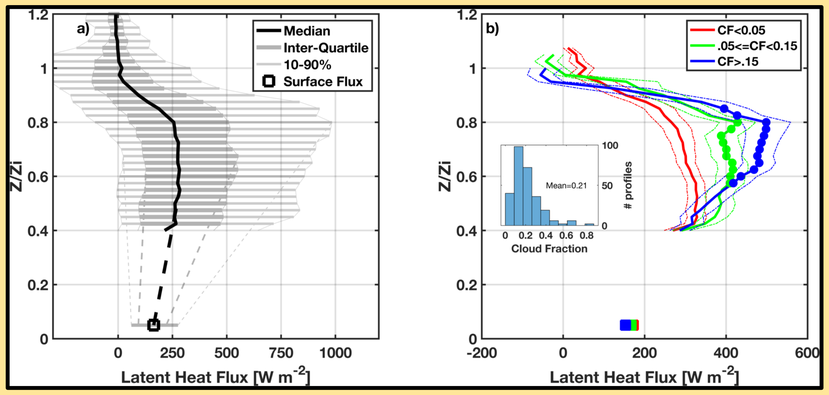

6. Diurnal cycle of latent heat flux

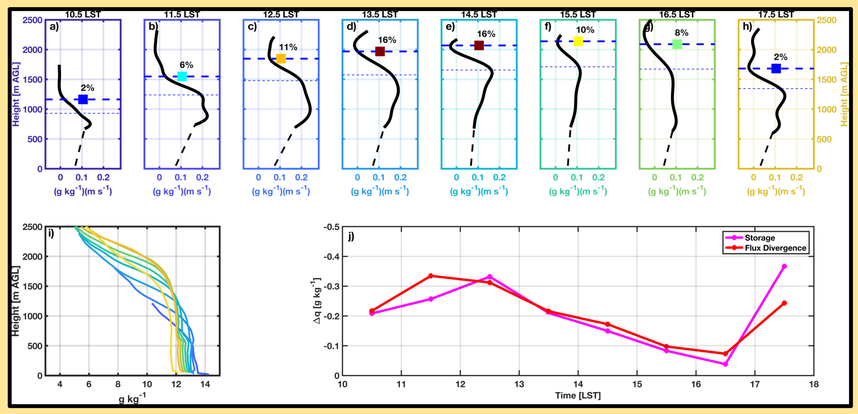

Figure 5. Diurnal cycle of kinematic latent heat flux profiles and CBL humidity budget. (a-h) Composite hourly latent heat flux profiles. Also shown are the CBL height (bold dashed), 0.8Z_i (light dashed), a line connecting the profile to the mean surface flux, and the average cloud fraction (labeled colored squares).The time is shown above each panel. (i) Time evolution of the mean mixing ratio profile, with colors corresponding to the axis coloring in a-h. (j) Storage (pink) and flux divergence (red) evolution for the composite day. Note the y-axis is reversed, such that more negative values indicate stronger drying.

- Fluxes peak near 0.8Z_i throughout the day.
- Minimum at Z_i
- Largest magnitude during peak cloudiness
- Strongest drying occurs during the late morning.

The CBL mixing ratio budget

$$\Delta\langle q \rangle = \left(\frac{\overline{(w'q')}_{sfc} - \overline{(w'q')}_{(.8Z_i)}}{0.8Z_i} \right) \Delta t$$

Shows that he change in storage (LHS) is closely approximated by the flux divergence (RHS) throughout the day.

7. Subcloud circulation and cloud base fluxes

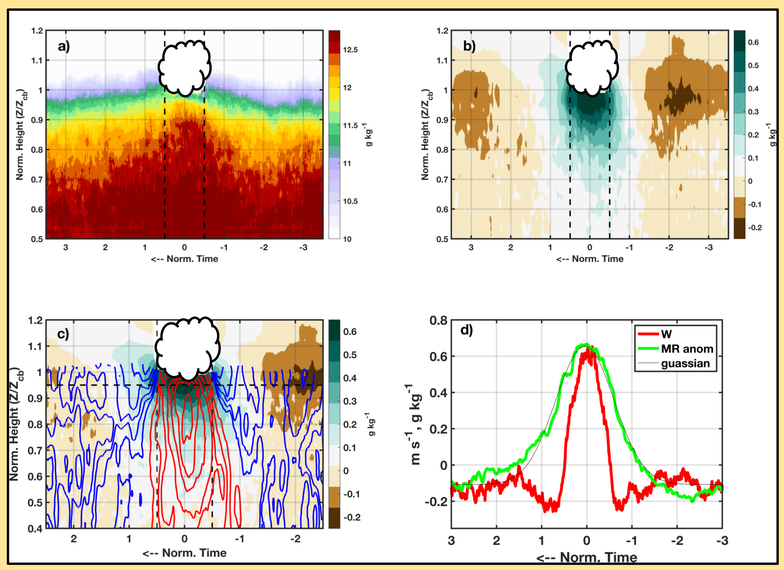

- Clouds linked to upward extrusion of high mixing ratio air.
- Water vapor anomaly most pronounced in upper CBL (>0.8Z_i)

- Clouds are linked to a coherent subcloud circulation.
  - Central updraft
  - Flanking downdrafts

- **Key finding**: The water vapor anomaly is systematically wider than the updraft.
  - Mechanically forced downdrafts have high mixing ratio air
  - Leads to a broad joint PDF of water vapor and vertical velocity

Figure 6. Composite subcloud and cloud-base properties. (a) Composite subcloud water vapor mixing ratio. (b) Composite subcloud mixing ratio anomaly. (c) Composite vertical velocity overlaid on the mixing ratio anomaly. (d) Cloud-base vertical velocity and mixing ratio anomaly. Also shown is a Gaussian fit to the mixing ratio data. All data are normalized to the cloud-base height and cloud duration, and centered on the cloud center time (i.e., 0).

8. Joint PDF of water vapor and vertical velocity

- The JPDF sampled in the upper CBL is broad and roughly isotropic, with a mix of wet-up, dry-up, dry-down, and wet-down observations.
- The JPDF during cloudy periods has larger vertical velocity and mixing ratio values, consistent with the increased flux during cloudy periods.

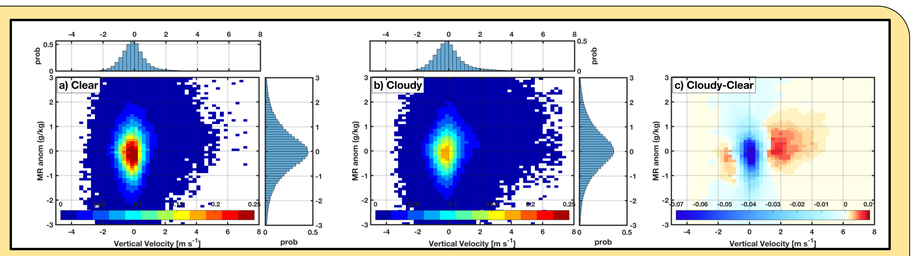

Figure 7. Joint probability density functions (JPDFs) for water vapor mixing ratio anomalies and vertical velocity in the upper CBL. (a) JPDF for clear periods. (b) JPDF for cloudy (cloud fraction>0.05) periods. (c) Difference between cloudy and clear JPDFs.

9. Summary

- Co-located Doppler and Raman lidar data are used to resolve the latent heat fluxes in the upper CBL
- Results expand on previous limited sampling of flux profiles, showing a quasi-linear increase in latent heat flux with height.
- These data also yield insights into the process level details of water vapor flux at cloud base, demonstrating systematic differences in the width of water vapor and vertical velocity anomalies

10. Acknowledgements

This work was supported by grant DE-SC0019124 from the Atmospheric Systems Research (ASR) program in the Office of Biological and Environmental Research, Office of Science, DOE.

We thank Rob Newsom for processing of the 10 sec Raman lidar data and Yunyan Zhang and Stephen Klein for input on the analysis.

Work in this poster is based on a manuscript submitted to the Journal of the Atmospheric Sciences.